# Numerical Investigation of Relative Contributions of $R_g$ Scattering and Incomplete Dissipation to $L_g$ Excitation[1]

Rong-Song Jih
Phillips Laboratory, PL/GPE
Hanscom AFB, MA 01731-3010

## Abstract

Numerous mechanisms have been proposed over the years to explain how the regional $L_g$ phase can be generated by nuclear explosions. Commonly quoted mechanisms include trapped *pS* phase, non-geometrical $S^*$, spall, multiple reflections of initial *P* rays, anisotropy, and various near-source, near-surface scattering processes. Recent observational studies (*e.g.*, Patton and Taylor, 1995) indicate that $R_g$ plays an important role in $L_g$ excitation for Yucca Flat explosions. Numerical experiments by Jih and McLaughlin (1995) readily demonstrate that rough topography and random heterogeneity can scatter significant $R_g$ energy into body waves. In this study, an additional $R_g$-to-$L_g$ conversion mechanism is presented and the relative effectiveness and importance of all three $R_g$-related mechanisms are examined.

It might be anticipated intuitively that the net effect of anelasticity in the surface layers is solely to reduce the amplitude of incident seismic waves. $R_g$ wave is particularly susceptible to such a mechanism since it is confined in the uppermost crustal layers. If the anelastic attenuating layer is only thick enough to dissipate the retrograde rolling near the surface, then the free surface would behave asymptotically like a fixed point. Beyond certain distance, the fundamental mode can no longer be sustained by such a waveguide, and accordingly any undissipated $R_g$ energy would have to propagate in other wave types or modes. Linear finite-difference calculations show that this process couples the undissipated $R_g$ energy into pure shear waves or higher modes, depending on the complexity of the structure. In terms of $R_g$-to-S to $R_g$-to-P ratio, this process appears to be more efficient than other near-surface $R_g$ scattering mechanisms. Furthermore, in this process, the $R_g$ spectrum is naturally imprinted onto the converted S waves, which could help to explain some recently observed spectral characteristics of $L_g$ waves.

For models embedded with shallow random heterogeneity, the RMS velocity fluctuation correlates very well with the $R_g$ transmission coefficient. For 1 Hz $R_g$, a 2%–5% variation in the velocity leads to an equivalent spatial Q value of several hundreds or larger, regardless which of the three commonly used random media is embedded. Rough topography typically results in a Q value ranging from 10 to 100, which is approximately equivalent to a random medium with a 10% (or larger) velocity variation. Incomplete dissipation of $R_g$ waves produces a very simple wave field, with almost all of the undissipated energy continues to propagate laterally towards the forward, and hence postcritical, directions. On the other hand, the scattering by shallow heterogeneity or rough topography would generate a rather complicated wave field, with a significant fraction of the scattered energy going downward steeply. Whichever of the three mechanisms is invoked, the S waves converted from $R_g$ always dominate the whole scattered field. The uppermost crust is highly heterogeneous, and in many places very attenuative and hilly as well. All of the three $R_g$-related mechanisms should therefore contribute to $L_g$ and coda excitation.

[1] This research was solely sponsored by the Air Force Technical Applications Center. **Key Words:** Rg, Lg, wave propagation, scattering, attenuation, finite-difference modeling.

**Project Objective**

The long-term objective of this project is to improve the fundamental understanding of seismic wave excitation and propagation. The full potential of linear finite-difference [LFD] method and other techniques shall be exploited in modeling various seismological problems directly related to a CTBT monitoring.

**Research Accomplished**

The first task of this project is to improve the capability of modeling $L_g$, $R_g$, $P_n$, $P_g$, and $S_n$ in complex geological / geophysical environments, using LFD or hybrid modeling tools. Following the LFD implementation of a pure $L_g$ wave packet (Jih, 1994), which is an ideal tool for investigating certain wave propagation phenomena (such as $L_g$ blockage), our research effort under this project has been re-directed to several subtasks:

[1] Use synthetic waveforms as an analysis aid to improve the phase-identification capability.[2]

[2] Explore the physical basis of high-frequency shear wave excitation in the vicinity of explosions due to cracking or pre-existing cracks.[3]

[3] Continue to investigate mechanisms responsible for explosion $L_g$ excitation.

This paper summarizes our results obtained to date under subtask [3], with emphasis placed on topics related to $R_g$. A new $R_g$–to–$L_g$ conversion mechanism is presented, and the relative effectiveness and importance of all three $R_g$–related mechanisms are reviewed.

Numerous mechanisms have been proposed over the years to explain how the regional $L_g$ phase can be generated by nuclear explosions. Commonly quoted mechanisms include trapped *pS* phase, non-geometrical $S^*$, spall, multiple reflections of initial *P* rays, anisotropy, and various near-source, near-surface scattering processes. Recent observational studies (*e.g.*, Patton and Taylor, 1995) indicate that $R_g$ plays an important role in $L_g$ excitation for Yucca Flat explosions. Numerical studies conducted at Teledyne Geotech and Phillips Laboratory (*e.g.*, McLaughlin and Jih, 1986, 1987; Jih, 1993ac, 1994) readily demonstrate that rough topography and random heterogeneity can scatter significant $R_g$ energy into body waves. However, in several cases only a fraction of the scattered energy would be favorably trapped in the crust as $L_g$ or $L_g$ coda, with more scattered energy lost to steeply going directions. In reality some additional $R_g$-to-$S$ mechanisms may have contributed to the observed $L_g$ signal as well.

It might be anticipated intuitively that the net effect of anelasticity in the surface layers is solely to reduce the amplitude of incident seismic waves. $R_g$ wave is particularly susceptible to such a mechanism since it is confined in the uppermost crustal layers. If the anelastic attenuating layer is only thick enough to dissipate the retrograde rolling near the surface, then the free surface would behave asymptotically like a fixed point. Beyond certain distance, the fundamental mode can no longer be sustained by such a waveguide, and accordingly any undissipated $R_g$ energy would have to propagate in other wave types or modes. Linear finite-difference calculations show that this process couples the undissipated $R_g$ energy into pure shear waves or higher modes, depends on the complexity of the structure (Figure 1). In terms of $R_g$–to–S to $R_g$–to–P ratio, this process appears to be far more efficient than other near-surface $R_g$ scattering mechanisms (Figure 5). Furthermore, in this process, the $R_g$ spectrum is

[2] See Kadinsky, Jih, Dainty, and Cipar (1995) of this issue.

[3] In progress with collaboration from A. Dainty and R. Blandford.

naturally imprinted onto the converted S waves, which could help to explain some recently observed spectral characteristics of $L_g$ waves. Figure 2 compares the propagation of $R_g$ waves incident upon an elastic and an attenuative basin models with identical velocity structures. Both the wave field snapshots (Figure 2) and the synthetic seismograms (Figure 3) clearly illustrate that $R_g$-to-$L_g$ conversion can be enhanced if the sedimentary rocks are shallow and strongly attenuative.

For the $R_g$ waves, rough topography could still be the strongest means of scattering (Jih, 1993abc). Scattering by random heterogeneity in the upper crust (*cf.* McLaughlin and Jih, 1987, and Jih, 1993b), is important in that random variations of velocity are virtually present in any type of crustal structure. McLaughlin and Jih (1987) made a comparison with Greenfield's (1971) P-coda observations (at teleseismic distance), and it was concluded that self-similar or Gaussian models with RMS velocity fluctuation between 7% and 15% in the uppermost 3 km of the crust can produce the observed P-coda/P power levels reported in Greenfield (1971). With the emphases of treaty-monitoring seismic research shifted to regional phases, $R_g$ scattering by shallow random heterogeneity needs to be re-examined in order to evaluate its importance and efficiency, with respect to other mechanisms, in exciting $L_g$ waves from explosions. In this study, a suite of forty five models embedded with shallow self-similar heterogeneous layer of varying randomness and thickness have been tested with LFD. Table 1 summarizes the propagation statistics we measured. Within 15% of velocity variation, the transmission, reflection, and the scattering loss all exhibit a linear relationship with the RMS velocity fluctuation. Models with thicker heterogeneities certainly associated with a stronger scattering and reflection, as well as a weaker transmission, as expected. However, the thickness appears to be less relevant than the RMS velocity variation (See Figure 4), primarily because $R_g$ scattering in the top 1 km is more important. These observations are also valid for random media with Gaussian or exponential correlations (see Frankel and Clayton, 1986, for the definitions of various random models).

**Conclusions and Recommendations**

There are at least three $R_g$-to-SV($L_g$) mechanisms: [A] scattering by shallow, random heterogeneity, [B] scattering by rough surface topography, and [C] incomplete dissipation by anelastic attenuation. Under this project, forward modeling is used to gain a better understanding of these three mechanisms. It is shown that, through extensive LFD modeling, each of these mechanisms can contribute to $L_g$ and coda waves from explosions. In terms of $R_g \to S$ / $R_g \to P$ power ratio, [C] is the most efficient one, followed by [B] and then [A]. $R_g$-to-S conversion systematically dominates the scattered wave field. In terms of equivalent spatial Q's, rough surface topography typically corresponds to a $Q_0$ in the range between 10 and 100 (Jih, 1993c), which is approximately equivalent to a self-similar random medium with 10% (or larger) RMS variation in the velocity. An RMS velocity fluctuation between 5% and 10% would correspond to a $Q_0$ value between 100 and 450 (Table 1). Stable shield regions have been reported to have an RMS velocity fluctuation less than 5%, which would yield a $Q_0$ larger than a few hundreds, regardless which type of random heterogeneity is considered. For all three types of random media that are commonly used in numerical studies with RMS velocity variation below 15%, all four measurable $R_g$ propagation statistics correlate extremely well with the RMS velocity fluctuation. Incomplete dissipation of $R_g$ waves produces a very simple wave field, with almost all of the undissipated energy continues to propagate laterally towards the forward, and hence postcritical, directions. On the other hand, the scattering by shallow heterogeneity or rough topography would generate a rather complicated wave field, with a significant fraction of the scattered energy going downward steeply.

An accurate prediction of the regional phases in areas of high proliferation concern requires a decent understanding of the attenuation/scattering mechanisms along the propagation paths. Synthetic seismograms are particularly useful for regions where earthquake or explosion data are not available. 2D numerical experiments, as described herein and in our previous studies, demonstrate that $R_g$ can be a significant contributor to the formation of $L_g$ and coda waves, in support of several observational studies. It would seem reasonable that, as 3D structure is taken into account, $R_g$'s possible role in $L_g$ excitation would only become more important. On a long term, however, extending 2D modeling capability to 3D is definitely useful, as it would add an extra level of realism and complexity to the earth's structures that we need to model. In particular, in order to quantify 3D effects of surface topographic irregularities, the operational 2D formulations of Neumann boundary conditions (Jih *et al.*, 1988) need to be expanded to a 3D version.

**References**

Frankel, A. and R. W. Clayton (1986), Finite-difference simulation of seismic scattering: implications for the propagation of short-period seismic waves in the crust and models of crustal heterogeneity, *J. Geophy. Res.*, **91**, 6465-6489.

Greenfield, R. J. (1971). Short-period $P-$wave generation by Rayleigh-wave scattering at Novaya Zemlya, *J. Geophys. Res.*, **76**, 7988-8002.

Jih, R.-S. (1993a). Directional excitation of $R_g$ due to ripple-fired explosions: a 2-dimensional finite-difference calculation, in *Proceedings of Numerical Modeling for Underground Nuclear Test Monitoring Symposium* (S. Taylor and J. Kamm, eds.), *Los Alsmos National Laboratory Report No. LAUR-93-3839.*

Jih, R.-S. (1993b). User's manual of FD2: a software package for modeling seismological problems with 2-dimensional linear finite-difference method, *Report TGAL-93-06,* Teledyne Geotech, Alexandria, VA.

Jih, R.-S. (1993c). Statistical characterization of rugged propagation paths with application to $R_g$ scattering study, *Report TGAL-93-07,* Teledyne Geotech, Alexandria, VA.

Jih, R.-S. (1994). Numerical modeling of crustal phase propagation in irregular waveguides, in *Proceedings of 16th PL/AFOSR Seismic Research Symposium* (J. Cipar, J. Lewkowicz, and J. McPhetres, eds.), *Report PL-TR-94-2217,* Phillips Laboratory, Hanscom AFB, MA, pp. 173-181 (ADA284667).

Jih, R.-S., K. L. McLaughlin and Z. A. Der (1988). Free boundary conditions of arbitrary polygonal topography in a 2-D explicit elastic finite difference scheme, *Geophysics,* **53**, 1045-1055.

McLaughlin, K. L. and R.-S. Jih (1986). Finite-difference simulations of Rayleigh wave scattering by 2-D rough topography, *Report AFGL-TR-86-0269,* Air Force Geophysics Laboratory, Hanscom AFB, MA (ADA179190).

McLaughlin, K. L. and R.-S. Jih (1987). Finite-difference simulations of Rayleigh wave scattering by shallow heterogeneity. *Report AFGL-TR-87-0322,* Air Force Geophysics Laboratory, Hanscom AFB, MA (ADA194961).

Patton, H. J. and S. R. Taylor (1995). Analysis of $L_g$ spectral ratios from NTS explosions: implications for the source mechanisms of spall and the generation of $L_g$ waves, *Bull. Seism. Soc. Am.*, **85,** 220-236.

| Table 1. Transmission/Reflection/Scattering Statistics of Self-Similar Models | | | | | |
|---|---|---|---|---|---|
| Model | T(1Hz) | R(1Hz) | 1-T-R | Q(1Hz) | $\gamma$ |
| 1km, 2% | 0.99 | 0.01 | 0.01 | 10172 | 0.000 |
| 2km, 2% | 0.98 | 0.01 | 0.01 | 8018 | 0.000 |
| 5km, 2% | 0.98 | 0.01 | 0.01 | 6710 | 0.000 |
| 10km, 2% | 0.98 | 0.01 | 0.01 | 6179 | 0.000 |
| 1km, 3% | 0.96 | 0.02 | 0.03 | 2000 | 0.001 |
| 2km, 3% | 0.95 | 0.02 | 0.03 | 1788 | 0.001 |
| 5km, 3% | 0.95 | 0.02 | 0.04 | 1646 | 0.001 |
| 1km, 4% | 0.92 | 0.03 | 0.06 | 931 | 0.001 |
| 1km, 5% | 0.86 | 0.04 | 0.10 | 548 | 0.002 |
| 2km, 5% | 0.85 | 0.04 | 0.11 | 502 | 0.002 |
| 5km, 5% | 0.84 | 0.04 | 0.12 | 473 | 0.002 |
| 10km, 5% | 0.84 | 0.04 | 0.12 | 457 | 0.002 |
| 15km, 5% | 0.83 | 0.04 | 0.12 | 451 | 0.002 |
| 1km, 6% | 0.80 | 0.06 | 0.14 | 363 | 0.003 |
| 1km, 7% | 0.73 | 0.07 | 0.20 | 258 | 0.004 |
| 1km, 8% | 0.66 | 0.09 | 0.25 | 192 | 0.005 |
| 1km, 9% | 0.58 | 0.10 | 0.31 | 147 | 0.007 |
| 1km, 10% | 0.51 | 0.12 | 0.38 | 116 | 0.009 |
| 2km, 10% | 0.47 | 0.11 | 0.42 | 105 | 0.009 |
| 5km, 10% | 0.45 | 0.11 | 0.44 | 99 | 0.010 |
| 10km, 10% | 0.45 | 0.11 | 0.44 | 99 | 0.010 |
| 15km, 10% | 0.45 | 0.11 | 0.44 | 98 | 0.010 |
| 1km, 11% | 0.43 | 0.13 | 0.44 | 92 | 0.011 |
| 1km, 12% | 0.35 | 0.14 | 0.50 | 75 | 0.013 |
| 1km, 13% | 0.28 | 0.16 | 0.56 | 61 | 0.016 |
| 1km, 14% | 0.22 | 0.17 | 0.61 | 51 | 0.020 |
| 1km, 15% | 0.16 | 0.18 | 0.66 | 42 | 0.024 |
| 2km, 15% | 0.13 | 0.17 | 0.71 | 37 | 0.027 |
| 5km, 15% | 0.12 | 0.17 | 0.72 | 36 | 0.028 |
| 10km, 15% | 0.13 | 0.16 | 0.71 | 38 | 0.026 |
| 15km, 15% | 0.13 | 0.16 | 0.71 | 38 | 0.026 |
| 1km, 16% | 0.11 | 0.19 | 0.70 | 35 | 0.028 |
| 1km, 17% | 0.08 | 0.20 | 0.72 | 30 | 0.034 |
| 1km, 18% | 0.05 | 0.21 | 0.74 | 25 | 0.040 |
| 1km, 19% | 0.03 | 0.22 | 0.76 | 21 | 0.048 |
| 1km, 20% | 0.01 | 0.22 | 0.76 | 17 | 0.058 |
| 2km, 20% | 0.01 | 0.23 | 0.76 | 15 | 0.066 |
| 5km, 20% | 0.01 | 0.23 | 0.77 | 14 | 0.069 |
| 10km, 20% | 0.01 | 0.23 | 0.76 | 15 | 0.066 |
| 15km, 20% | 0.01 | 0.24 | 0.75 | 17 | 0.060 |
| 1km, 21% | 0.01 | 0.23 | 0.77 | 14 | 0.070 |
| 1km, 22% | 0.00 | 0.23 | 0.76 | 12 | 0.081 |
| 1km, 23% | 0.00 | 0.24 | 0.76 | 11 | 0.088 |
| 1km, 24% | 0.00 | 0.24 | 0.76 | 11 | 0.091 |
| 1km, 25% | 0.00 | 0.24 | 0.76 | 10 | 0.097 |

T: transmitted power, R: reflected power, 1-T-R: scattering loss, $\gamma$ : attenuation coefficient.

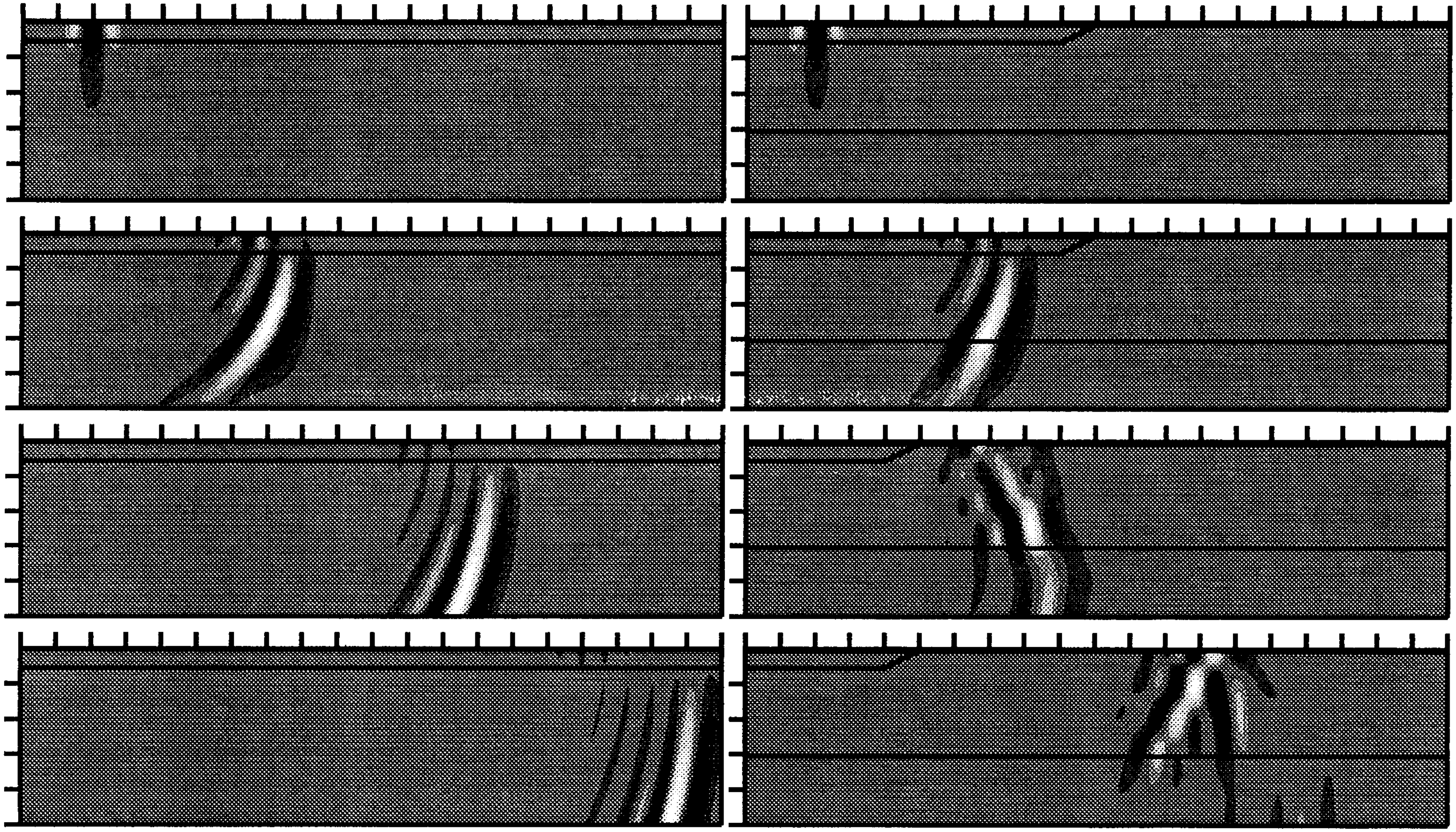

**Figure 1.** Snapshots of vertical wavefield of planar $R_g$ incident upon simple attenuative structures. In the case of an elastic half space overlain by a strong, shallow attenuative layer (left), the retrograde rolling near the surface is dissipated after certain distance. With the free surface behaves asymptotically like a fixed point, this waveguide could no longer support the fundamental mode. As a result, most of the undissipated $R_g$ energy is forced to propagate (in the forward direction) as shear waves. As the structure becomes more complex, the converted shear waves can easily couple into higher modes and contribute to $L_g$ and $L_g$ coda. Shown on the right is a model with a terminating attenuative layer on the top. Adding an extra layer (of higher velocity) to the model helps to trap the converted shear waves in the waveguide.

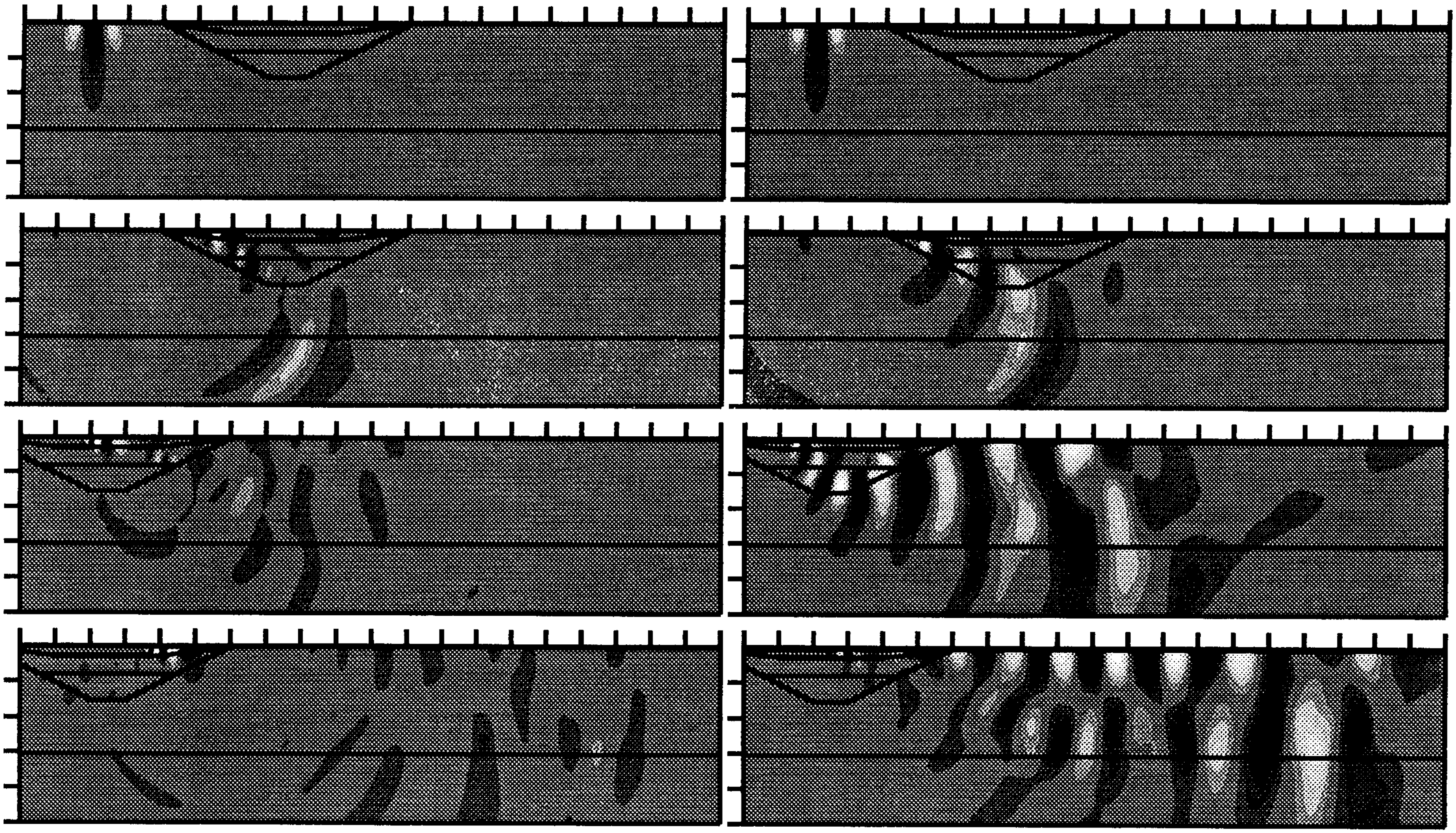

**Figure 2.** Snapshots of planar $R_g$ incident upon contained basin structures. In the elastic basin model (left), the low-velocity basin slows down the fundamental mode. Although the scattering at the basin edges removes some energy from the $R_g$ wave packet, the fundamental mode still retains the largest amplitude (See Figure 3). When the basin is replaced with depth-dependent low-Q materials (with the velocity unchanged), the fundamental mode is broken up, with the energy that tunneling through the deeper portion of the basin dominates the wavefield. This energy propagates as higher modes after passing through the basin.

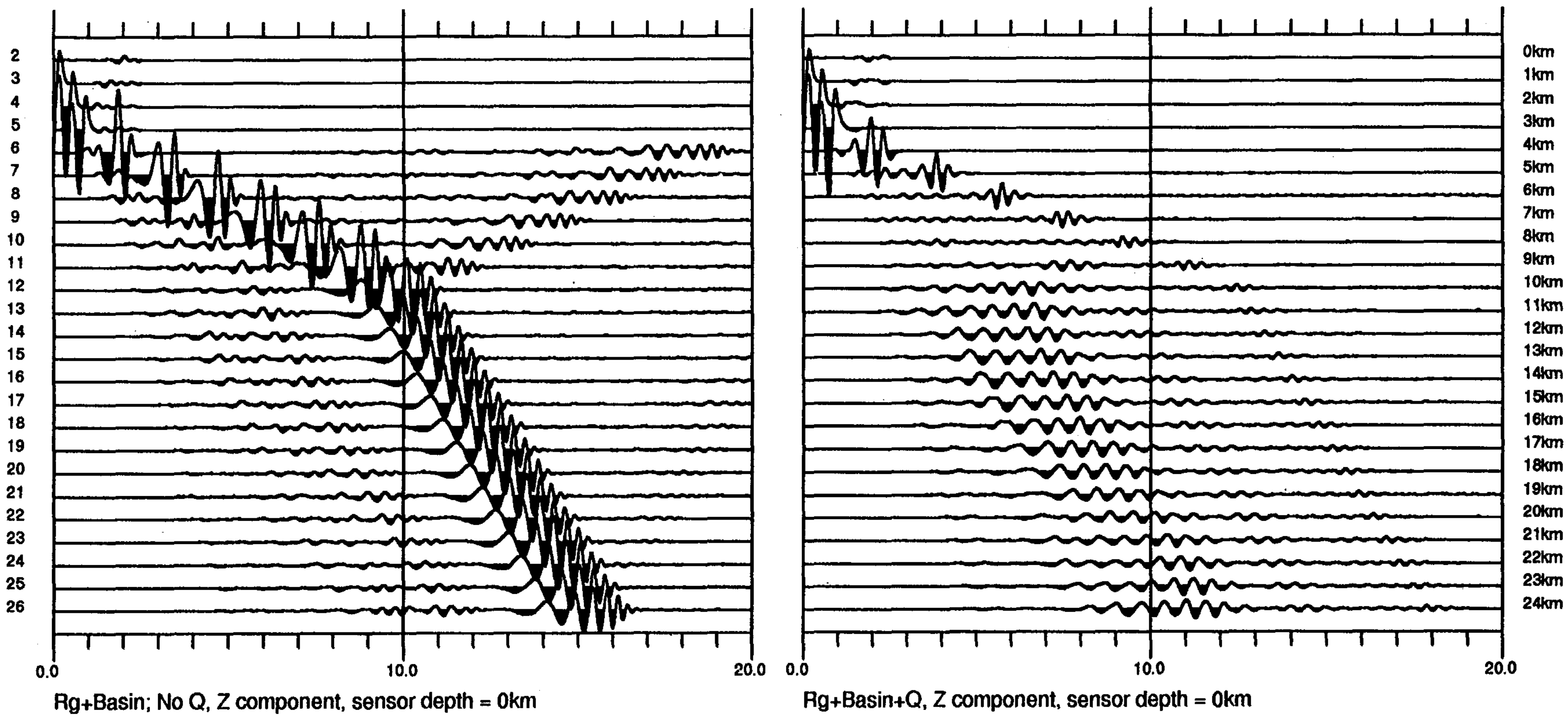


**Figure 3.** Synthetic seismograms, plotted in the same scale, for the two models shown in Figure 2. In the elastic basin model (left), the low-velocity sedimentary layers slow down the fundamental mode and cause significant backscattering at the basin edge. A fraction of the energy tunnels through (and under) the deeper layers of the basin and becomes higher modes, which travels ahead of the dominating fundamental mode. A little $R_g$ -to-P conversion is also visible. When the basin is replaced with depth-dependent low-Q material (with the velocities unchanged), the $R_g$ amplitude is reduced dramatically The higher modes become the dominant phase in the transmitted wave train. Forward $R_g$ -to-P conversion is enhanced as well. Note that the backscattering of $R_g$ at basin edges becomes negligible (in this scale).

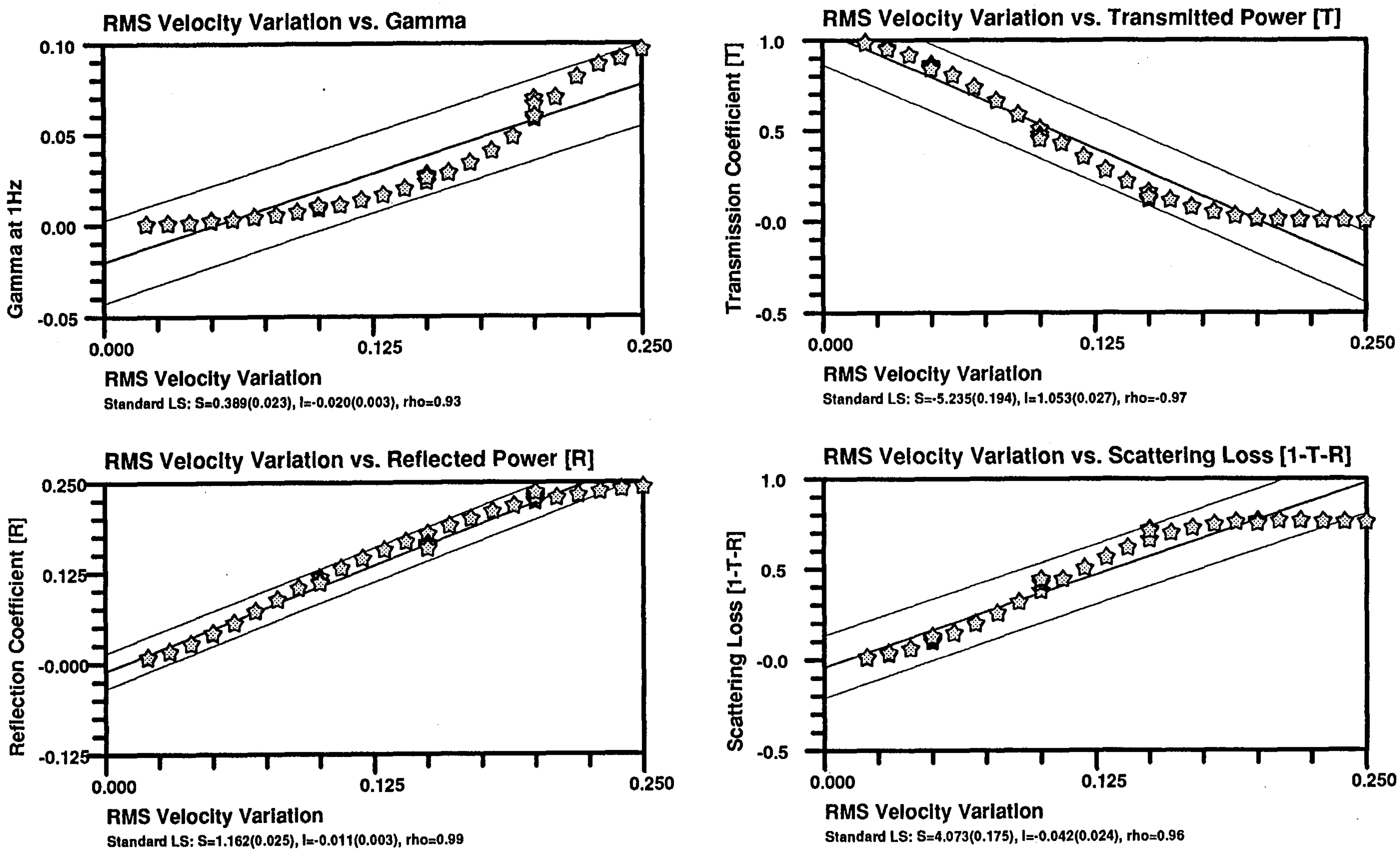


**Figure 4.** Regressing the attenuation coefficients [γ] (top left), transmitted power [T] (top right), reflected power [R] (bottom left), and scattering loss [1-T-R] (bottom right), respectively, on the RMS velocity fluctuation, σ, of 45 models with the thickness of the embedded self-similar shallow heterogeneous layer ranges from 1km to 5km. A 2%–5% variation in the velocity leads to an equivalent spatial Q value of 400 or larger for 1Hz $R_g$ phase. Models with stronger heterogeneities have larger γ's, stronger reflection, and smaller T's, as expected. The excellent linear fit (for up to 15%) suggests that general propagation statistics can be predicted with the RMS velocity variation alone.

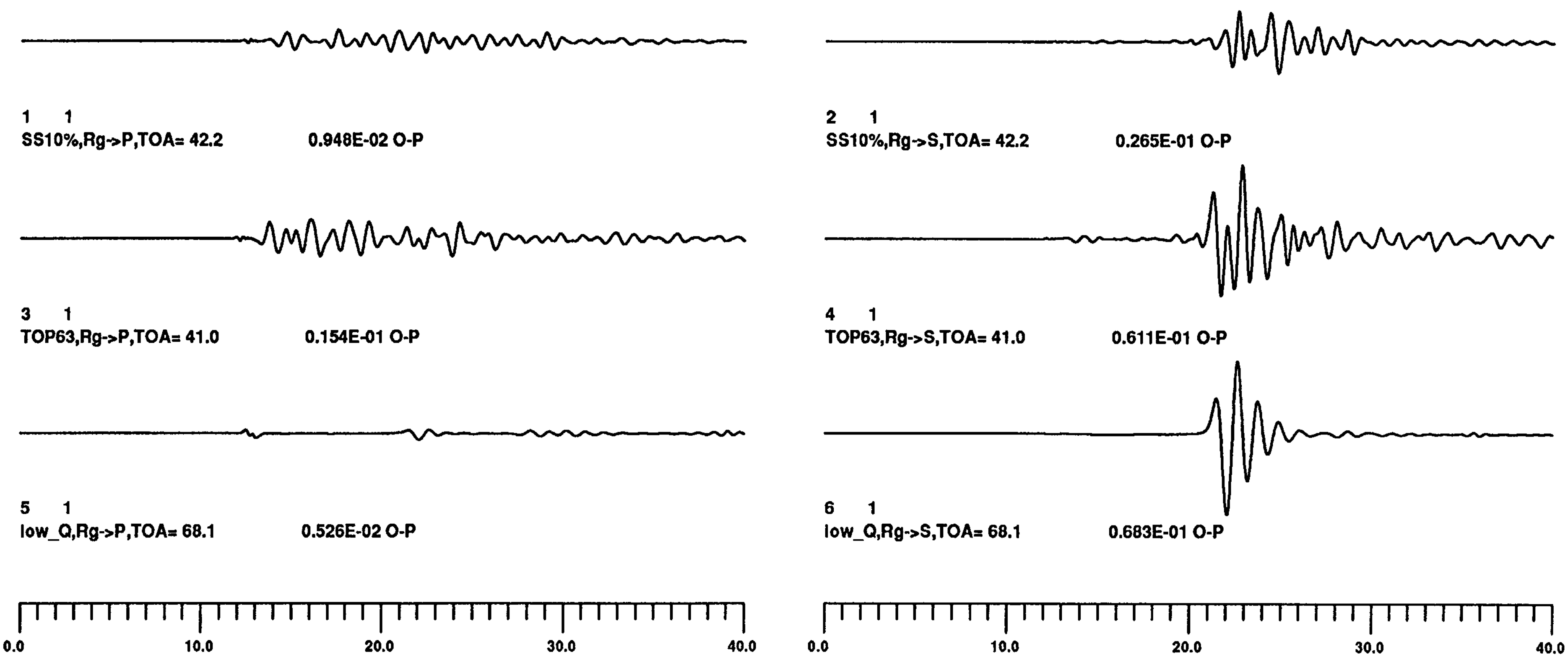


**Figure 5.** Comparison of LFD synthetic displacement seismograms of scattered body waves converted from $R_g$ due to three different mechanisms. Shown on the left and right are the converted P and S waves, respectively, recorded at a depth of 5 km. The take-off angle and the peak amplitude of the scattered rays are shown under each trace. The three heterogeneous structures being compared are (from top) [1] a half-space model embedded with self-similar shallow heterogeneity with 10% velocity fluctuation, [2] a half-space model overlain by a rough topographic profile, and [3] a half-space model overlain by a strongly attenuative layer. A pure $R_g$ wave packet was injected into the homogeneous portion of the grid to trigger the LFD calculations. In addition to the identical initial condition, other parameters (such as the grid size, the grid spacing, and the material properties of the bedrock) were also identical in these LFD simulations. Controlled numerical experiments using LFD are particularly convenient in isolating the effect of different mechanisms on $R_g$ (or other phases). In terms of $R_g \to S$ / $R_g \to P$ ratio or peak S-wave amplitude, incomplete dissipation of $R_g$ waves appears to be more efficient than the two scattering processes. Scattering by topography or heterogeneity would generate a much longer coda, however. For each of the three $R_g$ mechanisms investigated so far, $R_g \to S$ conversion is univocally stronger than that of $R_g \to P$.